Research Square

Preprints are preliminary reports that have not undergone peer review.
They should not be considered conclusive, used to inform clinical practice,
or referenced by the media as validated information.

Mogrol Protects Against Hepatic Ischemia–Reperfusion Injury by Preserving Mitochondrial Function Through PI3K/AKT Signaling

Wenzheng Ruan
The First Affiliated Hospital of Zhengzhou University
Ying Zhu
The First Affiliated Hospital of Zhengzhou University
An Zhao
The First Affiliated Hospital of Zhengzhou University
Haoran Fang
The First Affiliated Hospital of Zhengzhou University
Qiwen Yu
The First Affiliated Hospital of Zhengzhou University
Shengli Cao
shenglicao66@126.com
The First Affiliated Hospital of Zhengzhou University

Research Article

Keywords: Mogrol, Hepatic ischemia-reperfusion injury (HIRI), PI3K/AKT signaling pathway, Inflammation, Oxidative stress and Mitochondrial dysfunction

Posted Date: June 29th, 2026

DOI: https://doi.org/10.21203/rs.3.rs-9892316/v1

License: This work is licensed under a Creative Commons Attribution 4.0 International License.
Read Full License

Additional Declarations: No competing interests reported.

Mogrol Protects Against Hepatic Ischemia–Reperfusion Injury by Preserving Mitochondrial Function Through PI3K/AKT Signaling

Wenzheng Ruan [a,b,1], Ying Zhu [a,b,1], An Zhao [a,1], Haoran Fang [a,b], Qiwen Yu [c], Shengli Cao [a,*]

[a] Department of Hepatobiliary and Pancreatic Surgery, The First Affiliated Hospital of Zhengzhou University, Zhengzhou, Henan, 450052, China.

[b] Henan Key Laboratory for Digestive organ Transplantation, Zhengzhou, China.

[c] Department of Emergency Medicine, The First Affiliated Hospital of Zhengzhou University, Zhengzhou, Henan, 450052, China.

[1]These authors contributed equally to this work.

*Correspondence: Shengli Cao, Department of Hepatobiliary and Pancreatic Surgery, the First Affiliated Hospital of Zhengzhou University, 1 Jianshe East Road, Erqi, Zhengzhou, Henan, 450052, People's Republic of China.

Email: shenglicao66@126.com.

Abstract

Background: Hepatic ischemia–reperfusion injury (HIRI) is a common complication of liver surgery that significantly impairs clinical outcomes, and effective therapeutic strategies remain limited. Mogrol, a bioactive component derived from Siraitia grosvenorii, exhibits potent anti-inflammatory and antioxidant properties; however, its role in HIRI and the underlying mechanisms remain largely unexplored. **Methods:** To investigate the effects of Mogrol, both an in vivo hepatic I/R model in mice and an in vitro hypoxia/reoxygenation model using AML12 cells were employed. Mogrol was administered with or without the PI3K inhibitor LY294002. Liver function, histopathology, oxidative stress, inflammatory responses, and mitochondrial function

were assessed using biochemical assays, fluorescence staining, transmission electron microscopy, and ATP measurements. Transcriptomic analysis, molecular docking, and western blotting were performed to explore the underlying mechanisms. **Results:** Mogrol pretreatment significantly reduced serum ALT and AST levels, alleviated hepatic necrosis, suppressed oxidative stress and inflammatory responses, restored mitochondrial ultrastructure, stabilized mitochondrial membrane potential, inhibited mPTP opening, enhanced ATP production, and attenuated mitochondria-mediated apoptosis in both in vivo and in vitro models. These protective effects were partially reversed by LY294002. **Conclusion:** Mogrol mitigates HIRI, at least in part by activating the PI3K/AKT signaling pathway, highlighting its potential as a naturally derived candidate for liver protection.

Keywords: Mogrol, Hepatic ischemia-reperfusion injury (HIRI), PI3K/AKT signaling pathway, Inflammation, Oxidative stress and Mitochondrial dysfunction.

1. Introduction

Hepatic ischemia–reperfusion injury (HIRI) refers to tissue damage that occurs when blood flow to the liver is restored after a period of ischemia. HIRI is an unavoidable complication associated with liver trauma, surgical removal, transplantation, and systemic shock(1). Earlier research has demonstrated that HIRI is linked to calcium overload, oxidative stress, inflammation, mitochondrial damage, apoptosis, and ferroptosis(2-4). During periods of ischemia, most of the initial changes in hypoxic hepatocytes occur in the mitochondria. The absence of oxygen instantly stops electron flow, thereby impairing the respiratory chain. This leads to ATP depletion and accelerated glycolysis, triggering a homeostatic imbalance of intra- and extracellular inorganic ions and causing hepatocyte injury. During reperfusion, oxygen enters the bloodstream and produces toxic reactive oxygen species (ROS), which can be produced both intracellularly and extracellularly, with mitochondria being the

primary source in hepatocytes(3). Excessive ROS production during reperfusion increases mitochondrial membrane permeability and induces mitochondrial dysfunction, ultimately triggering apoptosis(5). In addition, ROS accumulation initiates a robust inflammatory cascade in hepatocytes, further exacerbating liver injury(6). At present, numerous approaches exist for treating HIRI, including surgical preconditioning, gene therapy, ischaemia time reduction and drug preconditioning(1, 7). Among them, drug preconditioning has become a major hotspot in recent years, so it is crucial to find drugs that can effectively reduce HIRI for clinical application.

Mitochondria play a central role in regulating cell survival and death during HIRI(8-10). Mitochondrial outer membrane permeabilization (MOMP) is a pivotal event in apoptosis(11, 12). Current research suggests two mechanisms for MOMP induction. First, hepatic ischemia-reperfusion injury induces an imbalance of intracellular and extracellular inorganic ions, leading to calcium overload(4), Elevated intracellular Ca^{2+} promotes mPTP opening, leading to loss of membrane potential and mitochondrial dysfunction. Ultimately, this leads to mitochondrial swelling and membrane rupture. In addition to calcium overload, several signals can turn on the mPTP. These signals include ROS, Changes in cellular pH levels, and specific medications(13). Another is induced by activated BAX and BAK(9). MOMP results in the release of cytochrome c. This release triggers the activation of the cysteine-dependent aspartate-specific proteases family, starting a cascade of cysteine asparaginase reactions that ultimately activate caspase-3, leading to apoptosis(12).

The process of HIRI involves several signaling pathways, including JAK/STAT3, Nrf2, PI3K/AKT, MAPK, and NF-κB(6, 14-17). Among them, PI3K/AKT signaling represents a key intracellular pathway that plays a central role in promoting cell survival, growth, and progression through the cell cycle(18). Recent evidence indicates that modulation of the PI3K/AKT signaling pathway, either through activation or inhibition, can mitigate HIRI(19-21). For example, Samar Rezq et al. demonstrated that rimonabant downregulates PI3K/Akt signaling, leading to reduced mTOR activity, increased autophagic processes, and attenuation of hepatic ischemia–reperfusion

injury(20); Mengting Zhan et al. revealed that Gas6/AXL enhances PI3K/Akt signaling, resulting in inhibition of ferroptosis and attenuation of HIRI(21), Moreover, Yanlu Liu et al. showed that coptisine activates the PI3K/Akt pathway, which contributes to reduced mitochondrial apoptosis and inflammatory responses in hyperuricemic nephropathy(22).

Native to southern China, Siraitia grosvenorii is a perennial herb widely recognized for its long-standing use as a natural sweetener and therapeutic agent in traditional Chinese medicine(23-25). Mogrol ($C_{30}H_{52}O_4$, **Figure 1**A for the chemical structure) is an aglycone of mogrosides, serving as the active ingredient of Siraitia grosvenorii. Emerging pharmacological research highlights the diverse bioactive properties of Mogrol, encompassing antioxidant, anti-inflammatory, antitumor, hypoglycemic, antitussive, and cardioprotective functions(23, 25-27) For example, Mogrol promotes AMPK pathway activation, which in turn suppresses inflammatory processes and mitigates ulcerative colitis. It can also induce apoptosis to inhibit lung cancer cell growth(23, 26). In addition, Feng Wang et al. revealed that Mogrol mediates cardioprotection by enhancing Ca^{2+} availability and Na^+/K^+-ATPase subunit 3 expression, while concurrently inhibiting apoptosis-related protein expression in cardiomyocytes and tissues(25). However, the potential therapeutic or preventive benefits of Mogrol on HIRI have yet to be verified.

Therefore, our study demonstrated the protective effect of Mogrol against HIRI and its underlying mechanism, aiming to provide a novel and effective strategy for alleviating such injury.

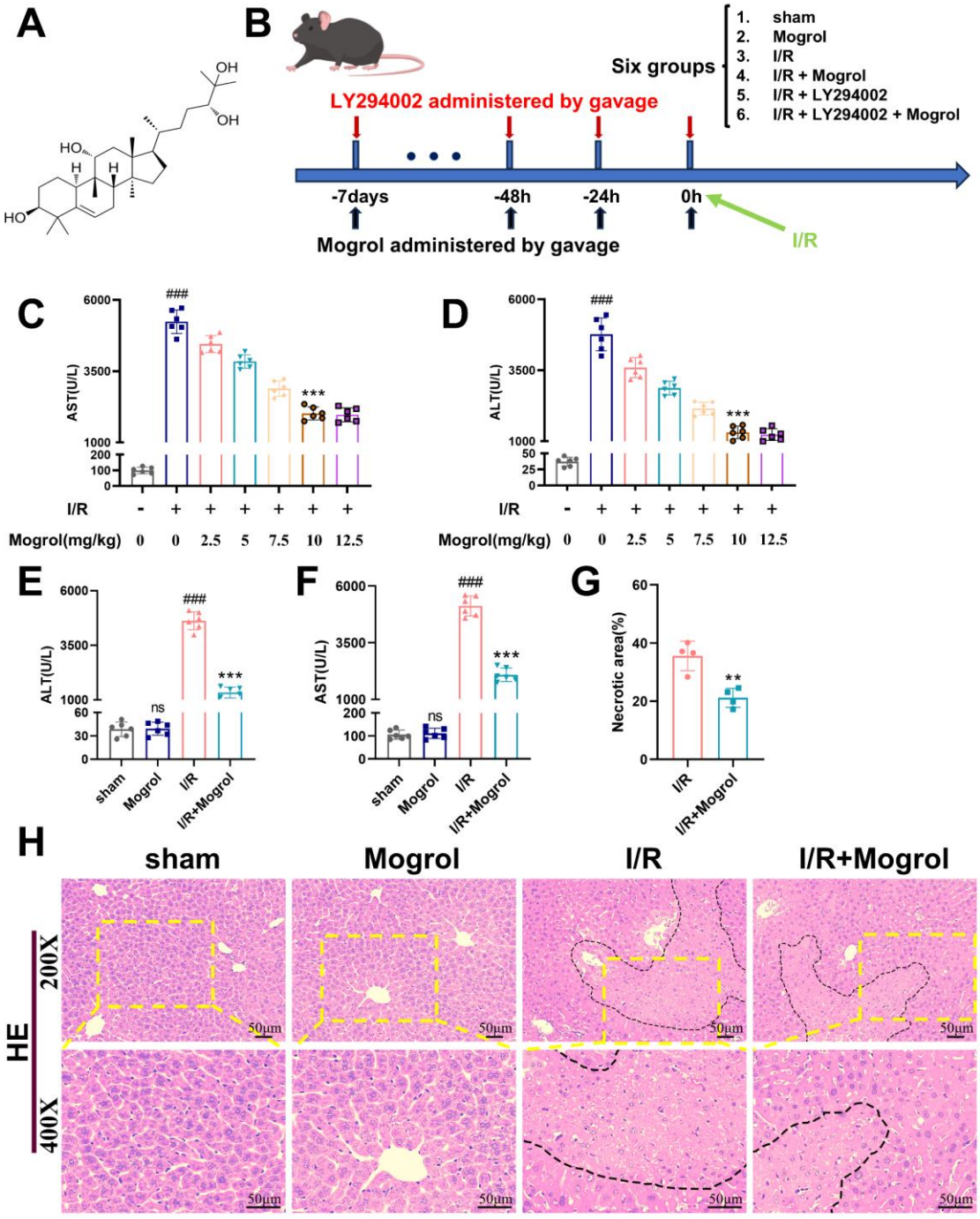


Figure1 Mogrol preconditioning alleviates HIRI. (A) Mogrol chemical structure. (B) Experimental grouping and flow chart. (C, D) Exploration of drug concentration. (E, F) Circulating ALT and AST levels measured after reperfusion. (G, H) H&E staining and quantification of necrotic area of liver tissue (necrotic areas are circled in black).

2. Materials and methods

2.1. Animals

Male C57 BL/6 J mice at 6-8 weeks of age were obtained from Huafukang Biotechnology (Beijing, China). All mice were maintained in a controlled and appropriate environment, with the temperature consistently maintained at 23±2°C and humidity ranging from 40% to 60%, while being exposed to a 12-hour light/dark cycle, and given adequate water and food during the feeding period. All animals were required to undergo one week of acclimatisation prior to the experiments and fasted for 12 h before surgery. All procedures were approved by the Ethics Committee of the First Affiliated Hospital of Zhengzhou University (Approval No. 2023-KY-0761-002).

2.2. Hepatic I/R injury model construction.

Mogrol (Product No. BP1837) was purchased from Chengdu Prefar Technology Co. Ltd (Chengdu, China) and LY294002 (HY-10108, Monmouth Junction, NJ, USA) was purchased from MCE (USA), dissolved in DMSO solution and diluted with saline. We divided the animal experiments into six groups (**Figure 1**B), which were the sham group, Mogrol group, I/R group, I/R+Mogrol group, I/R+LY294002 group, and I/R+LY294002+Mogrol group. Each group included six animals, all of them were administered by gavage, and were given for 7 consecutive days. Among them, Mogrol, I/R+Mogrol group was given Mogrol (10mg/Kg) drug treatment, but Mogrol group was not operated for hepatic ischemia-reperfusion injury, and sham and I/R groups were given equal volumes of saline and DMSO, but sham group was not operated for hepatic ischemia-reperfusion injury. To clarify the mechanism of Mogrol, LY294002 (50 mg/Kg, PI3K inhibitor) treatment was given again in the I/R group and the I/R+Mogrol group, respectively.

The liver ischaemia-reperfusion injury model was established as follows: mice were anesthetized with pentobarbital sodium (1%, 100 μL/10 g, Y0002194, Sigma

Aldrich), after laparotomy and exposure of the hepatic hilum, blood flow to the left and median lobes was occluded using a non-invasive vascular clip for 90 min to induce ischemia, followed by clip removal to allow reperfusion(28). Samples were collected six hours after reperfusion. Similar surgical maneuvers to those performed on the I/R group were performed on the sham and Mogrol groups, but no hepatic blood supply blockage occurred. Liver tissue samples and eye blood samples were collected after surgery. One portion of the liver tissue sample was quickly placed in liquid nitrogen and then transferred to a minus 80 degree freezer for cryopreservation. The other portion was preserved in a 10% formalin solution. After centrifuging the blood, retain the supernatant for subsequent testing.

2.3. Hematoxylin-Eosin (H&E) histological staining.

Hepatocellular necrosis was assessed through H&E histological examination. Liver tissue specimens were preserved in 10% neutral buffered formalin solution, subjected to dehydration processes and embedded in paraffin blocks. The paraffin-processed hepatic tissues were subsequently sectioned into 5-μm-thickness consecutive slices, which underwent staining procedures with hematoxylin (G1004, Servicebio, Wuhan, China) and eosin (BA-4024, Baso, Zhuhai, China). Photographic documentation of the processed glass slides was obtained through light microscopic imaging and archived.

2.4. Oxidative stress evaluation.

The collected hepatic tissue specimens and AML-12 cellular samples were combined with appropriate volumes of extraction medium, respectively. Samples were homogenized using an ultrasonic homogenizer. Subsequently, the homogenized sample was subjected to centrifugal separation at 4°C and 8,000 g for 10-minute duration. After centrifugation, the supernatant was collected and the protein concentration was measured. The concentrations of malondialdehyde (MDA), glutathione (GSH), and superoxide dismutase (SOD) were determined following protocols outlined in three

commercial kits (BC 0025, BC 5165, and BC 1175; Solarbio, Beijing, China). ROS levels in liver tissues were measured using dihydroethidium (DHE; Servicebio, Wuhan, China), while intracellular ROS were detected using a DCFH-DA staining kit (S0033S, Beyotime, Shanghai, China).

2.5. TUNEL staining of liver sections.

Hepatic tissue sections underwent staining following protocols specified in the TUNEL assay system (G1504, Servicebio, Wuhan, China). Subsequently, nuclear structures were labeled with DAPI (C1002, Beyotime, Shanghai, China). The processed hepatic tissue sections were examined using fluorescence microscopic techniques. Photographic documentation was preserved and positive cellular counts were enumerated utilizing ImageJ analytical software.

2.6. Immunofluorescent staining methodology.

Immunofluorescence staining was performed to detect Ly6G-positive cells. Paraffin-embedded sections underwent deparaffinization, rehydration, and antigen retrieval using EDTA solution. The tissue sections were subsequently blocked with 10% bovine serum albumin (BSA) for one-hour duration at 37°C temperature, followed by triple PBS washing procedures. immediately after, at 4°C temperature, the sections received overnight incubation with anti-mouse lymphocyte antigen 6 complex motif G antibody (Ly6G; GB11229; 1:200 dilution ratio; Servicebio, Wuhan, China). Post-PBS washing, the specimens were exposed to fluorescent secondary antibody treatment (GB21401, Servicebio, Wuhan, China) and maintained for one-hour period at ambient temperature. Ultimately, photographic documentation was obtained through fluorescence microscopic imaging.

2.7. Cellular cultivation and H/R experimental model.

AML 12 cellular lines were purchased from ProCell Life Science & Technology

(Wuhan, China) and cultured in DMEM/F12 medium (Solarbio, Beijing, China) at 37°C in a humidified incubator containing 5% CO_2 and 95% air. The cellular populations were monitored microscopically until they completely filled the field of view. Subsequently, subculturing procedures were performed. The cellular experimental design comprised four distinct groups: the Control group, Mogrol group, H/R group, and H/R+Mogrol group. Cells assigned to the control and Mogrol groups were cultured under standard conditions using complete medium. Cells in the H/R and H/R+Mogrol groups underwent cultivation in simulated hypoxic conditions for 12-hour periods within a 37°C constant-temperature tri-gas incubation system (1% O_2, 5% CO_2, and 94% N_2) utilizing glucose-free and serum-depleted DMEM/F12 medium (Solarbio, Beijing, China), subsequently receiving incubation in standard medium within incubation environments for six-hour reoxygenation periods. The Mogrol and H/R+Mogrol groups received Mogrol treatment (40μmol/L concentration) for 24-hour periods preceding experimental procedures. Equivalent volumes of saline solution were administered to Control and H/R groups.

2.8. Cellular viability evaluation assay.

AML12 cells were seeded into 96-well culture plates (4000 cells per well), allowed to adhere, pre-exposed to DMEM/F12 medium containing varying Mogrol concentrations for 24-hour periods, subsequently subjected to H/R treatment protocols, then incubated with DMEM/F12 medium supplemented with 10% CCK-8 reagent (C0041, Beyotime, Shanghai, China) for 2-hour duration. The cells underwent detection utilizing enzyme-linked detection instrumentation (Thermo Fisher).

Identical Mogrol concentrations received pre-treatment for varying temporal durations before experiencing hypoxic reoxygenation procedures. This was succeeded by hypoxic treatment for 12-hour periods, subsequently followed by reoxygenation for 6-hour duration. Finally, incubation with CCK-8 reagent was performed for detection analysis.

2.9. Reverse transcription quantitative PCR (RT-qPCR) analysis.

Total RNA was isolated from AML12 cells and liver tissues using TRIzol reagent (R1100, Solarbio, Beijing, China). Reverse transcription was performed using 1 μg of RNA, followed by quantitative PCR with SYBR Green Master Mix (SR1110, Solarbio, Beijing, China). Gene expression levels were normalized to β-actin and calculated using the 2^−ΔΔCt method. Primer sequences are listed in Table 1.

Table 1 list of primers

Gene	Primers
IL-1 β	5′-TGGACCTTCCAGGATGAGGACA-3′（Forward）
IL-1β	5′-GTTCATCTCGGAGCCTGTAGTG-3′（Reverse）
TNF-α	5′-GGTGCCTATGTCTCAGCCTCTT-3′（Forward）
TNF-α	5′-GCCATAGAACTGATGAGAGGGAG-3′（Reverse）
IL-6	5′-TACCACTTCACAAGTCGGAGGC-3′（Forward）
IL-6	5′-CTGCAAGTGCATCATCGTTGTTC-3′（Reverse）
IL-10	5'-GCTCTTACTGACTGGCATGAG-3'（Forward）
IL-10	5'-CGCAGCTCTAGGAGCATGTG-3'（Reverse）
β-actin	5′-GGCTGTATTCCCCTCCATCG-3′（Forward）
β-actin	5′-CCAGTTGGTAACAATGCCATGT-3′（Reverse）

2.10. Western blot.

Complete protein extraction from hepatic tissue specimens and AML12 cellular samples was accomplished utilizing RIPA lysis buffer system (R0010, Solarbio, Beijing, China). Protein quantification was established employing BCA assay methodology (PC0020, Solarbio, Beijing, China). The protein specimens underwent separation through SDS-PAGE electrophoresis and subsequent transfer onto polyvinylidene difluoride (PVDF) membrane substrates. The membrane substrates received overnight incubation with primary antibodies at 4°C temperature, followed by incubation with respective secondary antibody preparations. Protein signal detection was achieved utilizing imaging instrumentation (Bio-Rad) combined with ECL chemiluminescent detection system. ImageJ analytical software was employed for protein quantitative

analysis and statistical evaluation. The antibody specifications utilized are documented in Table 2.

Table 2 list of antibodies

Antibody	Cat No	Manufacturer	Dilution
PI3K	60225-1-Ig	Proteintech	1:5000
p-PI3K	17366	CST	1:1000
AKT	10176-2-AP	Proteintech	1:4000
p-AKT	66444-1-Ig	Proteintech	1:3000
Cleaved caspase3	9661	CST	1:1000
Bcl-2	R23309	ZENBIO	1:800
Bax	50599-2-Ig	Proteintech	1:4000
Cytochrome c	4272	CST	1:1000
β-actin	66009-1-Ig	Proteintech	1:10000
Goat Anti-Rabbit IgG(H+L)	SA00001-1	Proteintech	1:10000
Goat Anti-Rabbit IgG(H+L)	SA00001-2	Proteintech	1:10000

2.11. ATP detection, MMP and mPTP assay.

ATP levels in tissues and cells were measured using an ATP Content Assay Kit according to the manufacturer's instructions (A095-1-1, Jiancheng, Nanjing, China). Weigh the appropriate amount of tissue according to the 1:9 ratio. Add nine times the volume of cold, double-distilled water for ice-bath homogenization. Take the supernatant after centrifugation at 3500 g for 10 minutes at 4 °C, boil the mixture for 10 minutes, centrifugation was performed under the same conditions as above. Take the supernatant for testing and add the test solution according to the instructions. Measure the absorbance value.

Mitochondrial membrane potential (MMP) and mitochondrial permeability transition pore (mPTP) evaluations were conducted following manufacturer protocols supplied with respective assay systems (C2003S and C2009S; Beyotime, Shanghai, China).

2.12. Transmission Electron Microscopy (TEM).

Mouse liver tissue specimens underwent fixation with electron microscopy preservation solution and sectioning into 50-nm-thickness preparations. Following established procedural guidelines, the tissue sections received staining with uranyl acetate and lead citrate solutions. Subsequently, imaging was conducted and documented using electron microscopic equipment (Servicebio, Wuhan, China).

2.13. RNA sequencing and bioinformatics analysis.

Total RNA was prepared from the I/R and I/R + mogrol groups for RNA-seq analysis using TRIzol reagent. KEGG pathway enrichment was conducted and evaluated using Fisher's exact test, with a threshold of $p < 0.05$ for significance. KEGG annotations were retrieved from the KEGG database. The resulting RNA-seq data have been deposited in the GEO repository (GSE324365).

2.14. Molecular docking.

Ligand structures were initially obtained from the PubChem database and subsequently converted into three-dimensional forms using ChemOffice, followed by saving in mol2 format. Crystal structures of target proteins were downloaded from the RCSB PDB database and processed as receptor models. Structural preparation, including removal of solvent molecules and unnecessary ions, was performed in PyMOL, and the refined structures were retained in PDB format. Docking simulations were conducted using AutoDock Vina 1.5.6 to assess ligand–protein interactions. Prior to docking, ligands and receptors were further optimized with AutoDock Tools by adding hydrogen atoms, removing redundant components, and defining rotatable bonds. The docking region was defined according to the active site coordinates. Binding poses were ranked based on affinity scores, and the most favorable conformations were selected for subsequent analysis. Visualization of interactions between ligands and key residues was performed using Discovery Studio 2019 and PyMOL in both 2D and 3D

representations.

2.15. Statistical analysis.

All experimental data are presented as mean ± standard deviation (SD) values. Comparative analyses between two or multiple experimental groups were conducted utilizing independent samples t-testing or one-way analysis of variance (ANOVA) procedures. Complete statistical evaluations were executed using GraphPad Prism analytical software (version 7.0; GraphPad Software, Inc.). $P < 0.05$ was considered as statistically significant, and each experimental procedure was replicated a minimum of three times. Figure legend description： Ns, not significant vs. sham/Control; $^{\#}p < 0.05$, $^{\#\#}p < 0.01$, $^{\#\#\#}p < 0.001$ vs. sham/Control (Figure1- Figure6); $^{\#}p < 0.05$, $^{\#\#}p < 0.01$, $^{\#\#\#}p < 0.001$ vs. I/R (Figure7- Figure8); $*p < 0.05$, $**p < 0.01$, $***p < 0.001$ vs. I/R/H/R; $*^{\#}p < 0.01$ vs. I/R+Mogrol.

3. Results

3.1. Mogrol pretreatment attenuates I/R-induced liver injury.

Dose optimization was performed in animal experiments. Treatment with 10 mg/kg significantly attenuated the increase in serum ALT and AST levels induced by I/R injury, whereas no additional reduction was observed at 12.5 mg/kg. Based on these findings, 10 mg/kg was chosen for further studies (**Figure 1**C, D). Serum transaminase levels were further evaluated. Compared with the sham group, ALT and AST levels were markedly elevated in the I/R group, indicating severe liver injury. No obvious changes were observed in the Mogrol-alone group (**Figure 1**E, F). In contrast, Mogrol treatment significantly decreased serum ALT and AST levels in the I/R+Mogrol group, suggesting partial restoration of liver function (**Figure 1**E, F). Histological assessment was conducted using H&E staining to reflect liver injury. Hepatic architecture was well preserved in the sham and Mogrol groups, with no obvious histological damage. In contrast, extensive hepatocellular necrosis was observed in the I/R group (**Figure 1**H).

Similar to the changes in serum aminotransferases, the I/R+Mogrol group significantly reduced the area of necrosis in the tissues (**Figure 1**G, H). Our study demonstrated that Mogrol pretreatment can effectively alleviate I/R-induced liver injury.

3.2. Mogrol pretreatment reduces oxidative stress and inflammatory responses induced by I/R.

During HIRI, reactive oxygen species (ROS) generation occurs both intracellularly and extracellularly, especially within the mitochondria of cells(3). Given the central role of ROS in oxidative stress, we examined ROS accumulation in liver tissues by DHE staining to evaluate whether Mogrol pretreatment could attenuate I/R-induced oxidative injury. Our findings revealed that ROS levels remained minimal and approximated physiological levels in sham and Mogrol treatment groups; conversely, ROS levels exhibited substantial elevation in the I/R group and demonstrated significant reduction following Mogrol preconditioning administration (**Figure 2**A, B). Simultaneously, we quantified additional oxidative stress biomarkers, encompassing MDA, SOD, and GSH, employing ELISA methodology. Consistent with the ROS results, Mogrol preconditioning decreased concentrations of the lipid peroxidation terminal product MDA and restored antioxidant capacity, as reflected by increased SOD activity and GSH content (**Figure 2**C-E). Moreover, our examination of inflammation-associated markers demonstrated substantial reduction in Ly6g-positive cellular infiltration numbers within the I/R+Mogrol group relative to the I/R group (**Figure 2**F, G). Additionally, expression of pro-inflammatory mediators IL-6, IL-1β, and TNF-α exhibited notable decreases, whereas concentrations of the anti-inflammatory mediator IL-10 showed significant elevation within the I/R+Mogrol group (**Figure 2**H-K). These observations indicate that Mogrol demonstrates substantial antioxidative and anti-inflammatory properties in hepatic ischemia-reperfusion injury pathology.

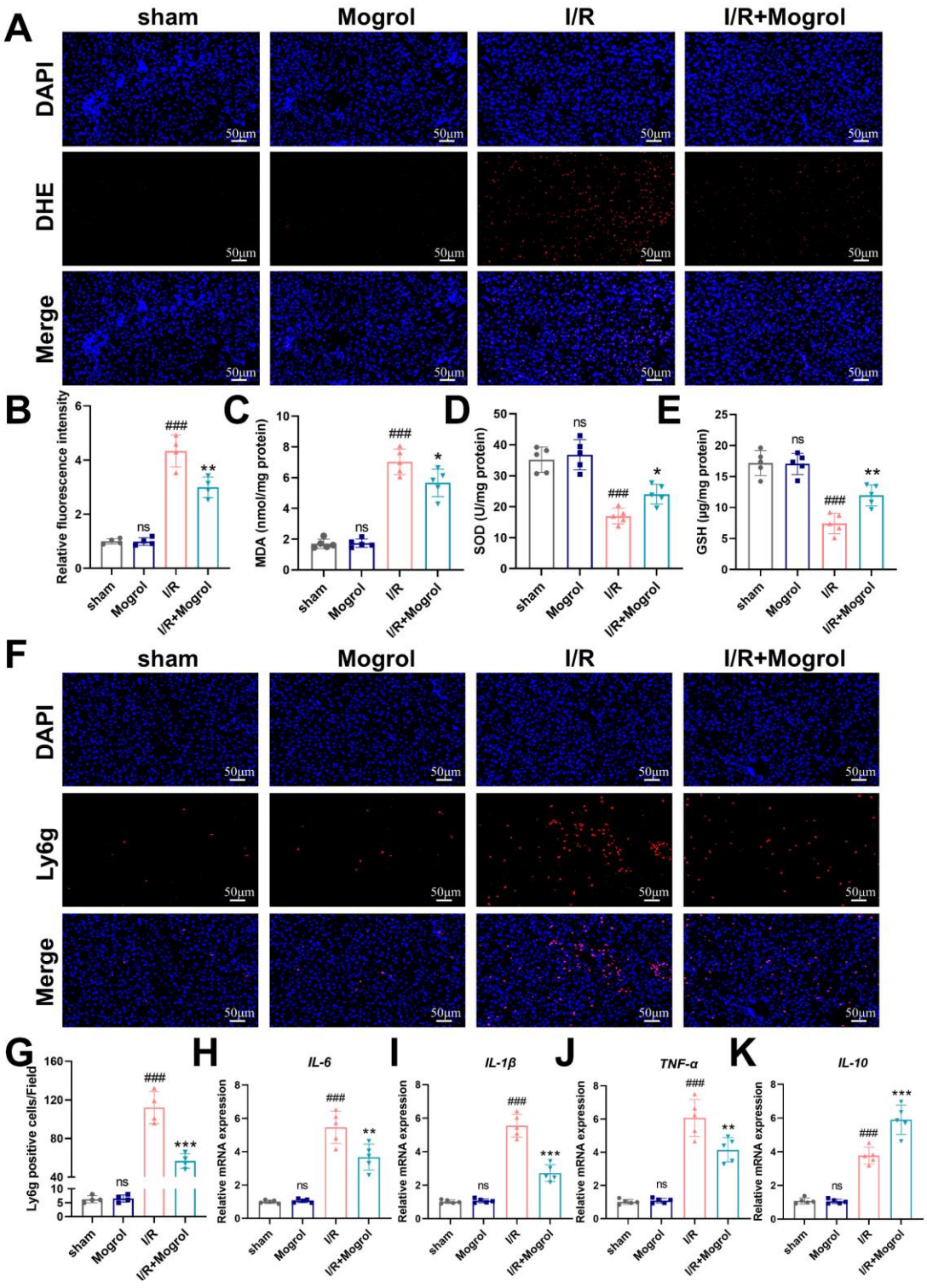


Figure2 Mogrol pretreatment mitigated oxidative stress and inflammation during HIRI. (A, B) DHE-based ROS detection and fluorescence intensity quantification in liver sections. (C, D, E) Biochemical evaluation of MDA, SOD, and GSH in liver tissues. (F, G) Ly6G staining with quantitative evaluation. (H, I, J, K) Liver mRNA abundance of IL-6, IL-1β, TNF-α, and IL-10 determined by RT-qPCR.

3.3. Mogrol pretreatment attenuates I/R-induced mitochondrial injury and apoptosis.

Oxidative stress induced by HIRI leads to permeabilization of the outer mitochondrial membrane, which results in a permeability shift in the mitochondrial membrane, leading to mitochondrial damage and mitochondria-mediated apoptosis(4, 12, 13). Consequently, the subsequent analysis focused on the examination of mitochondria-related morphological changes and apoptosis-related indicators. The morphological structure of mitochondrial damage is characterized by a variety of manifestations, including mitochondrial swelling; mitochondrial cristae structure breakage, reorganization, and change from laminar structure to fragmentation; mitochondrial vacuolation; mitochondrial membrane rupture, partial fusion, and complete disappearance. Transmission electron microscopy (TEM) analysis revealed that the mitochondrial structure in the sham and Mogrol groups exhibited near-normal characteristics, including an intact mitochondrial membrane structure, clearly visible cristae structure, and high matrix density. Within the I/R experimental cohort, despite preservation of mitochondrial membrane structural integrity, the mitochondrial cristae architecture became disrupted and vanished. The matrix electron density diminished and evident structural compromise occurred. Conversely, mitochondria within the I/R+Mogrol group displayed moderate structural compromise; the membrane architecture remained preserved, whereas the cristae structure exhibited fragmentation patterns (**Figure 3**A). Furthermore, tissue ATP content evaluation demonstrated that ATP concentrations were substantially diminished in the I/R group. Nevertheless, the I/R+Mogrol group manifested significant ATP content enhancement compared to the I/R group (**Figure 3**D).

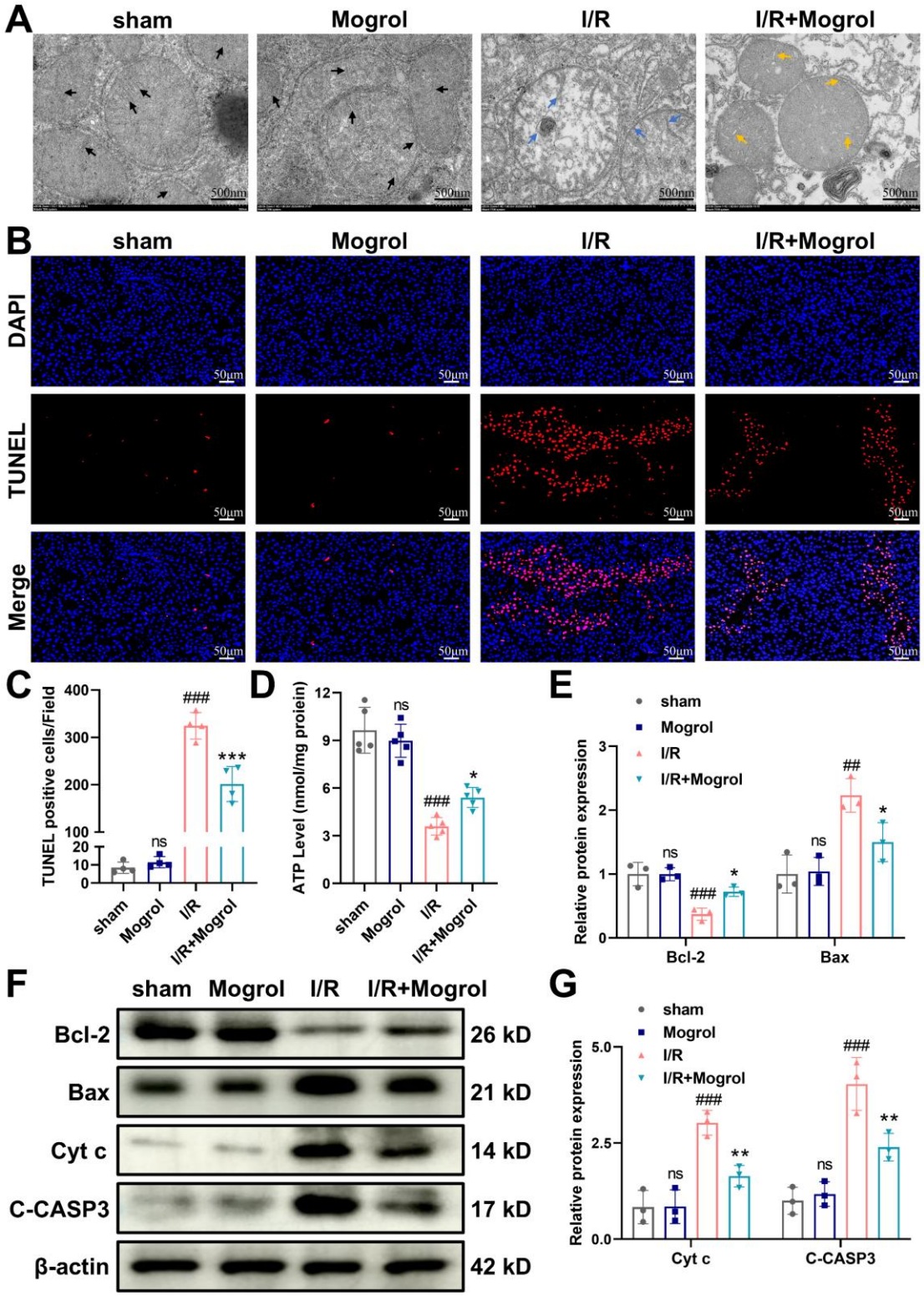


Figure3 Mogrol pretreatment reduces the damage caused to mitochondria and apoptosis by I/R. (A) The morphological structure of mitochondria under electron microscopy (Black arrows denote normal mitochondria; blue arrows mark mitochondrial damage with loss of organisation of the cristae structure; and orange arrows represent mild mitochondrial damage with fragmentation of the cristae structure). (B, C) Detection and statistical assessment of TUNEL-positive cells in liver

tissue. (D) ATP levels in liver tissue. (E, F, G) Immunoblotting results and semi-quantitative analysis for Bcl-2, Bax, Cyt c, and C-CASP3.

Subsequently, we investigated apoptosis-associated parameters. TUNEL staining outcomes revealed that the I/R+Mogrol group was capable of substantially mitigating the enhanced apoptotic levels triggered by I/R (**Figure 3**B, C). Follow-up analyses indicated that the I/R+Mogrol group demonstrated decreased elevated levels of Bax and cleaved caspase-3 proteins induced by I/R, alongside enhanced Bcl-2 protein expression levels through Western blot investigations (**Figure 3**F). cytochrome c represents a crucial protein in mitochondria-dependent apoptotic pathways, and our findings indicated that cytochrome c protein expression was markedly elevated in the I/R group, which was alleviated in the I/R+Mogrol group (**Figure 3**E-G).

3.4. Mogrol pretreatment alleviates H/R-induced AML12 cell injury.

To investigate the potential protective effect of Mogrol on AML12 cells, an AML12 cell H/R model was constructed. To detect cellular activity, a CCK-8 assay was performed on drug concentration gradients and time gradients of pretreatment. The results indicated that the addition of 40 μmol of Mogrol had the highest relative cellular activity, and there was no significant change in cellular activity when exceeding this concentration (**Figure 4**A). Similarly, the relative cellular activity was the highest when pretreated for 24 hours, and there was no significant change in cellular activity when exceeding this time point (**Figure 4**B). Consequently, Mogrol (40 μmol) prophylactic treatment for 24-hour duration was chosen for subsequent experimental investigations. In line with the animal experiments, Mogrol treatment shifted the inflammatory response toward a less activated state (**Figure 4**C-F). Mogrol was additionally determined to decrease MDA and ROS concentrations, as well as enhance GSH concentrations and SOD enzymatic activity (**Figure 4**G-J). Furthermore, mitochondrial functional experimental outcomes revealed diminished MMP and enhanced mPTP activation following H/R exposure. Remarkably, Mogrol preconditioning ameliorated the membrane potential reduction triggered by H/R and prevented the mPTP activation induced by H/R (**Figure 4**K, L and **Figure 5**A). Simultaneously, ATP evaluation

demonstrated that Mogrol preconditioning elevated ATP concentrations in response to H/R-induced cellular damage (**Figure 5**D). Ultimately, flow cytometric analysis and Western blot findings further confirmed Mogrol's inhibitory impact on mitochondria-dependent apoptotic pathways. Specifically, flow cytometric evaluation revealed substantial apoptotic rate reduction in the H/R+Mogrol cohort relative to the H/R cohort (**Figure 5**B, C). Western blotting further revealed that Mogrol shifted the apoptosis-related protein profile toward cell survival (**Figure 5**E-G). Therefore, Mogrol has been demonstrated to mitigate H/R-induced inflammatory responses, oxidative stress, and mitochondrial apoptosis, thereby providing protective benefits.

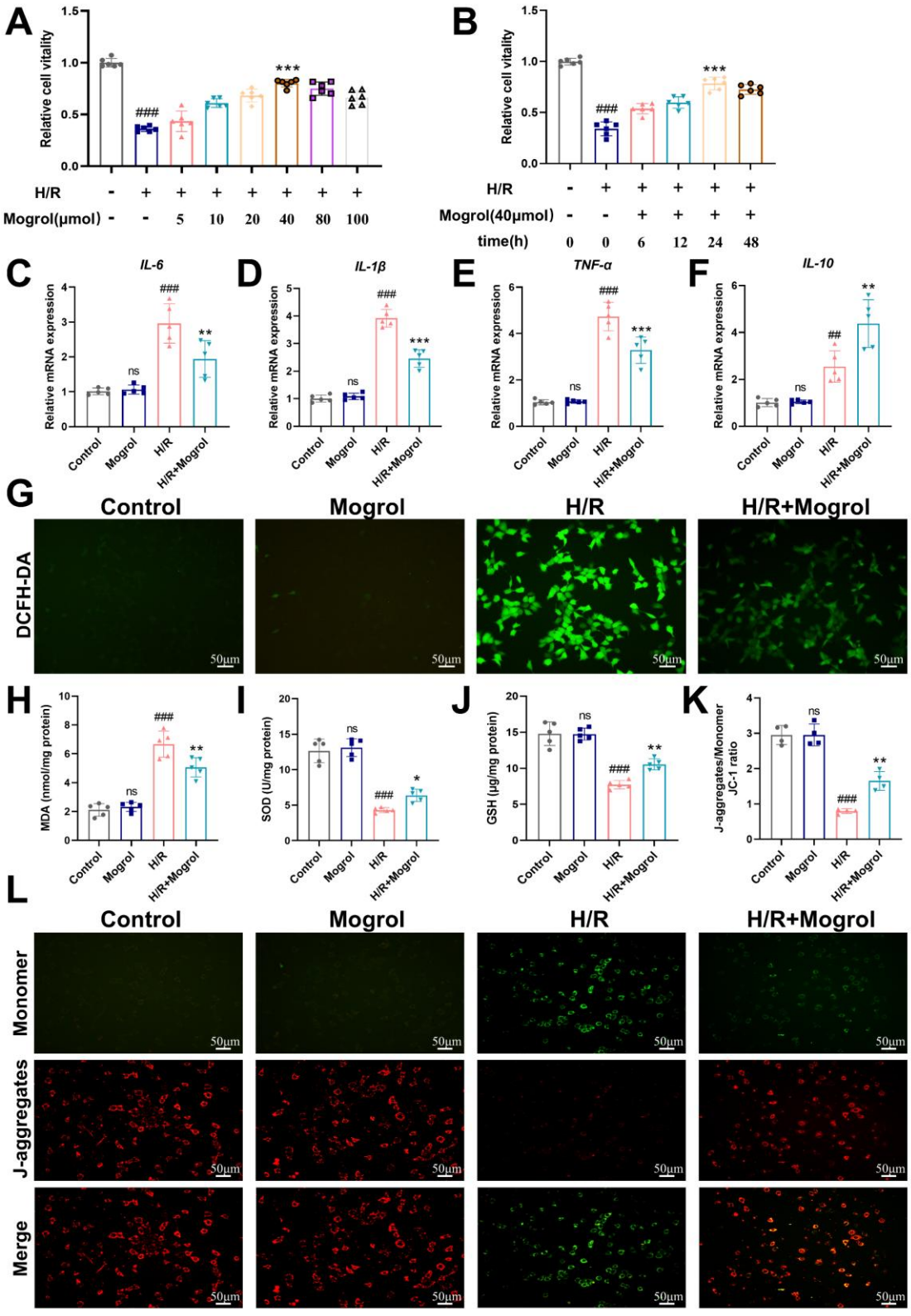


Figure4 Mogrol pretreatment protects AML12 cells against H/R-induced injury. (A, B) Effects of Mogrol dosage and pretreatment time on AML12 cell viability. (C, D, E, F) Expression profiles of inflammatory cytokines, determined by RT-qPCR. (G) DCFH-DA staining used to visualize ROS accumulation in AML12 cells. (H, I, J) Quantitative analysis of oxidative stress-related indicators in AML12 cells. (K, L) Mitochondrial

membrane potential measurement and statistical evaluation.

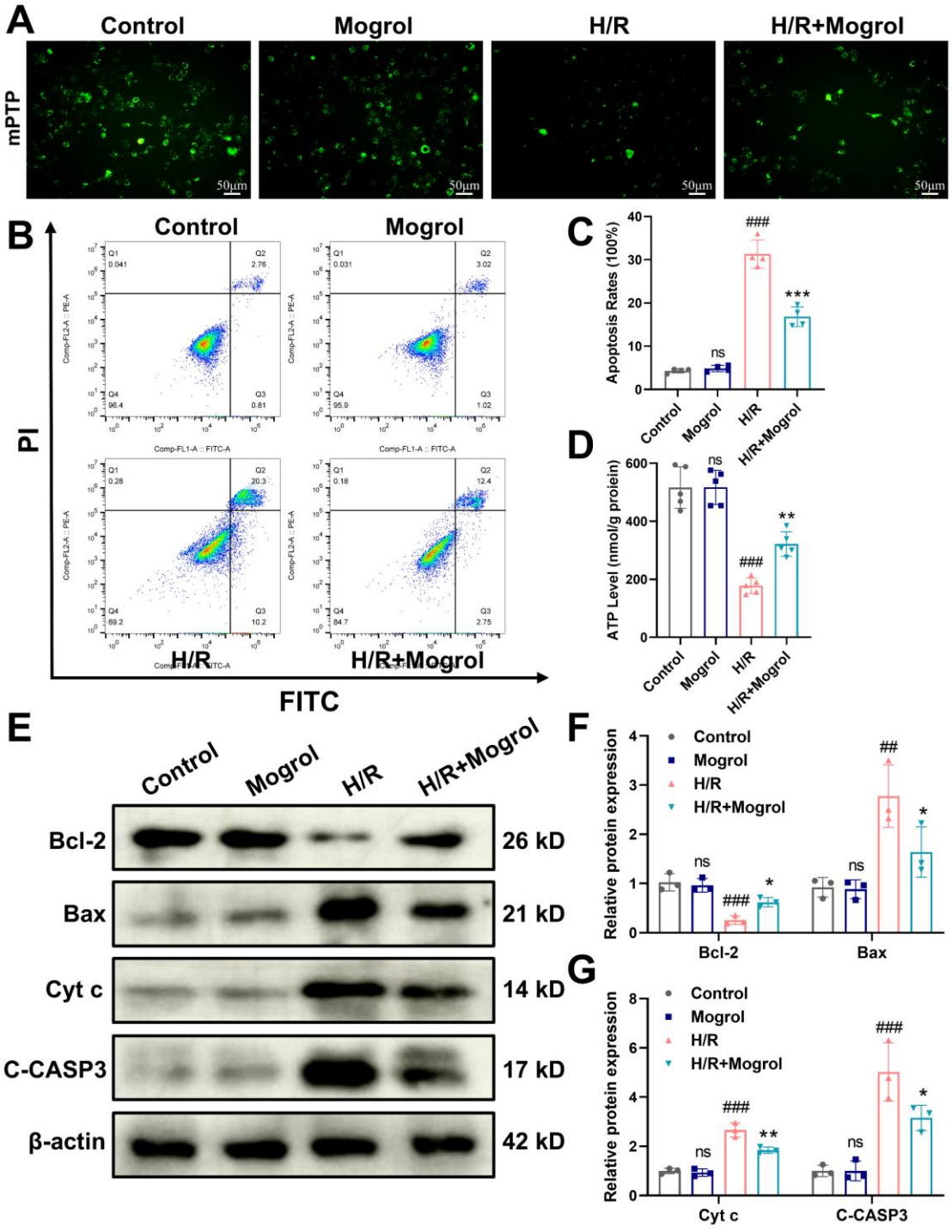


Figure5 Mogrol pretreatment protects AML12 cells against H/R-induced injury. (A) Mitochondrial Permeability Transition Pore (mPTP) Detection in AML12 cells. (B, C) Apoptosis analysis by flow cytometry. (D) ATP level Detection in AML12 Cells. (E, F, G) Protein expression and relative quantitative analysis of Bcl-2, Bax, Cyt c, and C-CASP3 in AML12 cells.

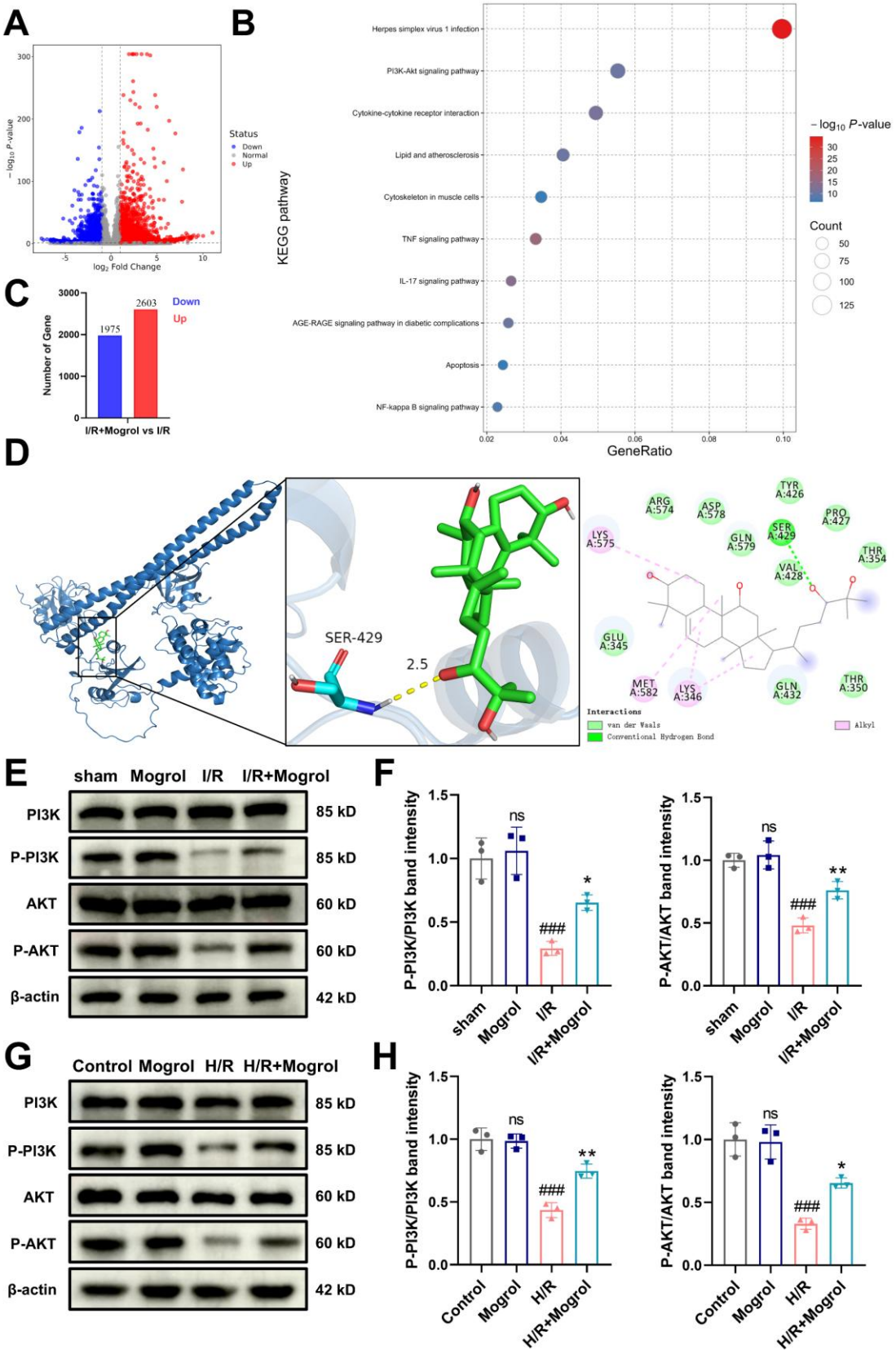


Figure6 Integrated transcriptomic, docking, and immunoblotting analyses of the PI3K/AKT axis after Mogrol treatment. (A, C) Volcano plots and distribution of upregulated and downregulated genes. (B) KEGG analysis. (D) Molecular docking of Mogrol to PI3K p85 subunit. (E, F) Immunoblotting bands and semi-quantitative

analysis of PI3K, phosphorylated PI3K, AKT, and phosphorylated AKT in hepatic samples. (G, H) Immunoblotting bands and semi-quantitative analysis of the same pathway-related proteins in AML12 cells.

3.5. Mogrol pretreatment activates the PI3K/AKT signaling pathway.

It has been established that multiple signaling cascades become activated throughout hepatic ischemia-reperfusion injury pathogenesis, wherein the PI3K/AKT signaling cascade demonstrates substantial importance(21, 29-31). Subsequently, we aimed to clarify the potential mechanisms underlying Mogrol's protective properties during HIRI. Transcriptomic sequencing analysis demonstrated the quantity of genes exhibiting up- and down-regulation through volcano plot visualization (**Figure 6**A, C); Enrichment analysis identified the PI3K/AKT signaling pathway as a key pathway involved in HIRI. (**Figure 6**B). Following this, molecular docking experiments were conducted, and it was found that Mogrol stably binds to the PI3K p85 subunit with a binding energy of -8.0 kcal/mol. This finding indicates a strong binding ability between the two (**Figure 6**D). Finally, the pathway underwent validation through protein immunoblotting experimental procedures. The I/R+Mogrol cohort demonstrated substantial enhancement in PI3K and AKT phosphorylation concentrations relative to the I/R cohort (**Figure 6**E, F). Furthermore, comparable outcomes were achieved in cellular experimental investigations (**Figure 6**G, H). In conclusion, the current findings suggest that Mogrol preconditioning activates the PI3K/AKT signaling cascade in hepatic I/R as well as in AML12 cellular H/R models.

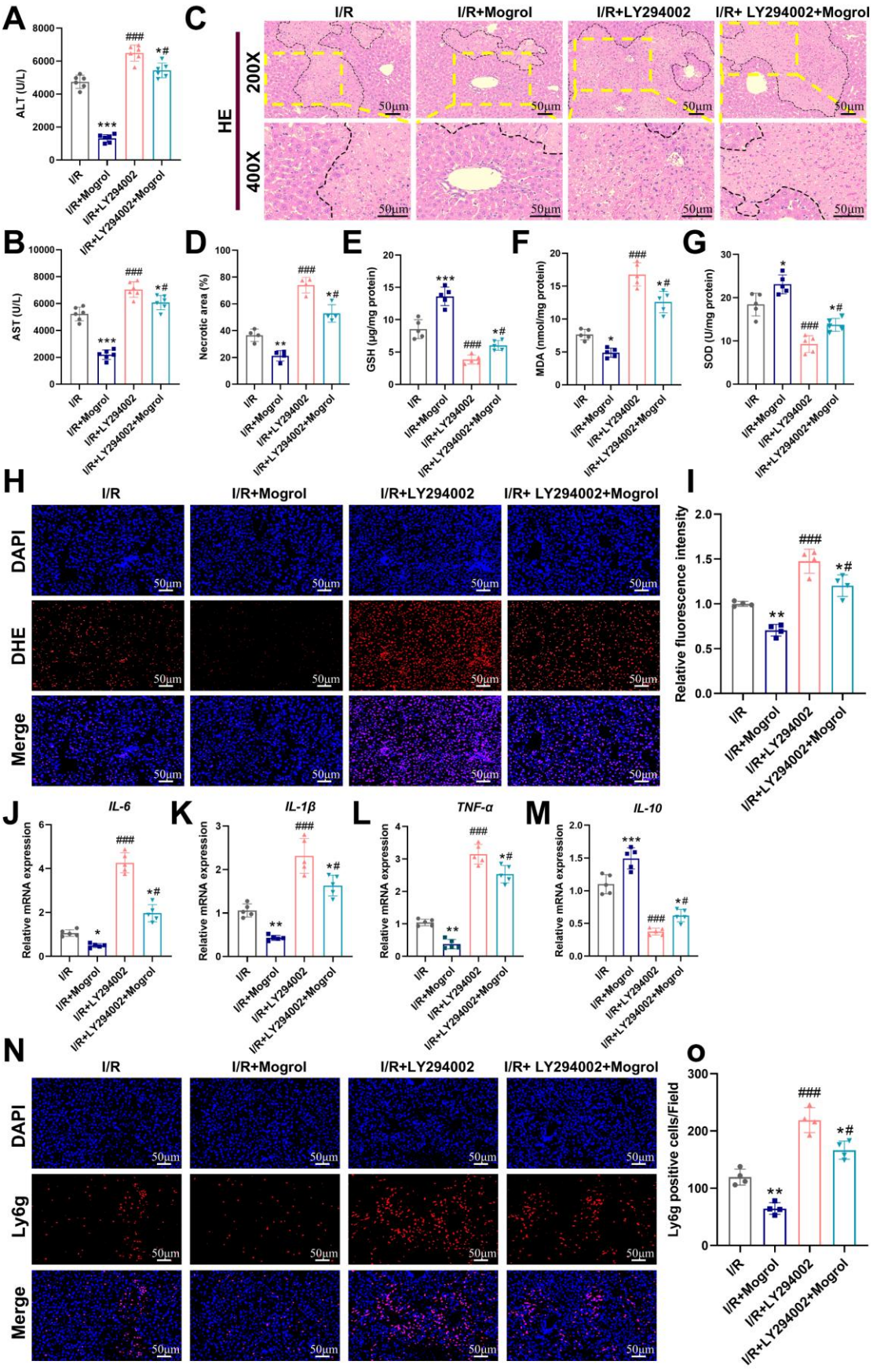


Figure7 LY294002 intervention partially reverses the effects of Mogrol on hepatic I/R

injury. (A, B) Circulating liver enzyme levels measured after reperfusion among different experimental groups. (C, D) H&E staining of liver tissues with statistical assessment of necrotic regions marked by black outlines. (E, F, G) Biochemical evaluation of MDA, SOD, and GSH in hepatic samples. (H, I) Visual analysis of ROS through DHE staining. (J, K, L, M) RT-qPCR-based assessment of inflammation-related transcript expression. (N, O) Ly6G staining.

3.6. Mogrol alleviates HIRI by activating the PI3K/AKT signaling pathway.

We next tested the dependence of Mogrol on PI3K/AKT signaling by introducing LY294002. Western blot analysis confirmed that LY294002 suppressed phosphorylation of PI3K and its downstream target AKT, verifying pathway inhibition in the I/R model (**Figure 8**E). Under I/R conditions, Mogrol reduced serum transaminase release and alleviated histological necrosis, whereas LY294002 produced the opposite trend (**Figure 7**A-D). When LY294002 was combined with Mogrol, the improvement in liver function and tissue morphology was less pronounced than that observed with Mogrol alone (**Figure 7**A-D). Similar changes were found in markers of oxidative stress and inflammation, including MDA, SOD, GSH, ROS, inflammatory cytokines, and Ly6G staining (**Figure 7**E–O). In addition, analogous outcomes were observed in terms of mitochondrial impairment and apoptosis induction. For instance, relative to the I/R group, Mogrol-treated mice displayed better-preserved mitochondrial ultrastructure, higher hepatic ATP levels, and attenuated apoptotic responses (**Figure 8**A-I). Nevertheless, LY294002 co-treatment weakened the ability of Mogrol to counteract I/R-induced mitochondrial injury and apoptotic signaling (**Figure 8**A-I). Thus, the PI3K/AKT pathway appears to be closely involved in the protective action of Mogrol against HIRI.

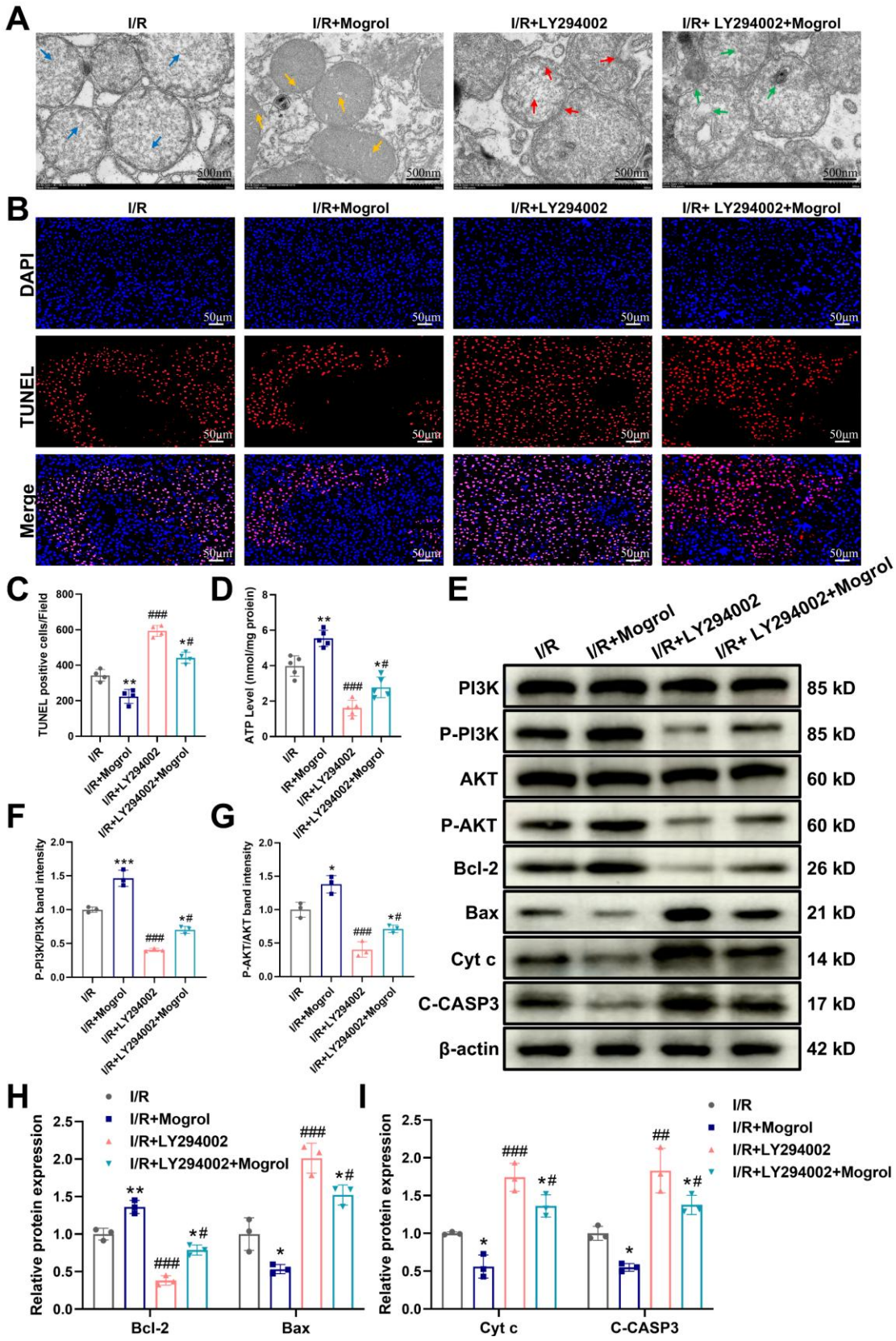


Figure8 Mitochondrial ultrastructure, apoptotic status, ATP production, and PI3K/AKT-related protein changes under LY294002 treatment. (A) The morphological structure of mitochondria under electron microscopy (Blue arrows represent mitochondrial damage with loss of organisation of the cristae structure; orange arrows

represent mild mitochondrial damage with fragmentation of the cristae structure; red arrows and green arrows indicate severe damage, where red arrows represent partial or complete rupture of the membrane structure, while green arrows indicate distortion and partial rupture of the membrane structure). (B, C) Detection and statistical evaluation of TUNEL-positive cells in liver tissue. (D) ATP level in liver tissue. (E, F, G, H, I) Immunoblotting results with semi-quantitative analysis for PI3K, phosphorylated PI3K, AKT, phosphorylated AKT, Bcl-2, Bax, Cyt c, and C-CASP3.

4. Discussion

HIRI is an adverse event that is unavoidable following liver surgery. It leads to abnormal liver function and failure, which seriously affects the prognosis of patients(32, 33). Mechanistically, HIRI mainly involves oxidative stress, inflammatory cascade, calcium overload, autophagy, mitochondrial damage, and apoptosis(1, 4, 33, 34). To date, considerable attention has been directed toward pharmacological agents, antioxidant-based interventions, and stem cell therapies as candidate strategies for reducing HIRI(34). In the present work, we utilized both animal and cellular models to investigate the protective role of Mogrol in HIRI. The results demonstrated that Mogrol administration effectively alleviated liver damage, enhanced cell survival, and mitigated oxidative stress, inflammatory responses, and mitochondrial impairment. Further mechanistic analyses indicated that activation of the PI3K/AKT axis played an important role in mediating these effects. Notably, pharmacological blockade of PI3K using LY294002 weakened the protective actions of Mogrol, supporting the critical involvement of this pathway in mediating its effects (**Figure 9)**.

Liver injury severity is commonly evaluated based on biochemical indicators of liver function and histopathological analysis(35). In this research, following pretreatment with Mogrol, we observed a reduction in serum transaminase levels, such as ALT, AST, alongside a decrease in necrotic region of the liver.

During the reperfusion phase, the reacquisition of oxygen by tissue leads to lipid peroxidation, which in turn generates substantial amounts of ROS within the mitochondria of hepatocytes. Cellular oxidative stress arises from dysregulation of ROS homeostasis, characterized by excessive production relative to clearance, which

can subsequently damage cellular membranes, mitochondria, and other macromolecules(34, 36, 37). Common endogenous antioxidants include GSH and SOD. The reduced glutathione is essential for eliminating free radicals in the body(34). This study evaluated the effects of mogrol pretreatment on oxidative stress in mouse liver and AML12 cells subjected to ischemia–reperfusion and hypoxia–reoxygenation. The experimental approach involved the measurement of MDA and ROS production, along with the assessment of GSH and SOD activities. The results obtained from this study demonstrated that Mogrol pretreatment led to a significant attenuation of oxidative stress, as evidenced by a decrease in ROS and MDA production, and an increase in GSH and SOD activities. Extensive research has shown that the significant generation of ROS during the reperfusion stage activates macrophages, leading them to release significant quantities of inflammatory mediators. This process has been shown to further exacerbate cell and tissue damage(38). Han Liang et al. discovered that Mogrol can alleviate ulcerative colitis by mediating the AMPK signaling pathway and thus ameliorating the condition(23). Furthermore, Varun Jaiswal et al. observed the anti-inflammatory properties of Mogrol in vivo and vitro experiments(39). Our findings indicate that Mogrol reduced the expression of pro-inflammatory cytokines (IL-6, IL-1β, and TNF-α) while increasing IL-10 levels in both hepatic I/R and H/R models. In addition, infiltration of Ly6G-positive cells was significantly decreased.

Mitochondria are crucial in energy generation, ROS generation, calcium balance, and the regulation of cell survival during HIRI(40). During the ischaemic phase, a lack of energy supply to cells and impaired ion pump function can lead to an imbalance of inorganic ions inside and outside the cell. This can cause calcium overload and lead to mitochondrial damage(4). A great deal of ROS is generated during reperfusion, which damages the mitochondrial membrane(36, 41). Damage to the mitochondria, as described above, leads to depolarisation of the membrane, opening of the mPTP, a decrease in MMP and MOMP(13) Furthermore, the protein Bax that promotes apoptosis, which belongs to the Bcl-2 family, facilitates mPTP opening in mitochondria. Under normal conditions, Bcl-2 and Bax combine to create a heterodimer that

suppresses Bax's pro-apoptotic activity. During apoptotic signaling, Bax translocates to the mitochondrial membrane and promotes mPTP opening, resulting in Ca^{2+} and H^{+} accumulation within the mitochondrial matrix. This disrupts mitochondrial membrane potential and increases membrane permeability, thereby facilitating the release of cytochrome c into the cytoplasm and activating the caspase cascade, ultimately leading to apoptosis(12, 13, 22, 41). Jing Huang et al.'s study pointed out that damage to the structure and function of mitochondria significantly contributes to liver ischemia-reperfusion injury(42). Our study also found that Mogrol pre-treatment significantly mitigated mitochondrial damage during liver I/R, restored MMP levels and closed the mPTP. It also decreased the protein expression of Bax, cytochrome c and cleaved caspase-3, while simultaneously increasing Bcl-2 expression. These effects suppressed the mitochondrial-mediated apoptotic pathway, thus providing a protective effect on the liver.

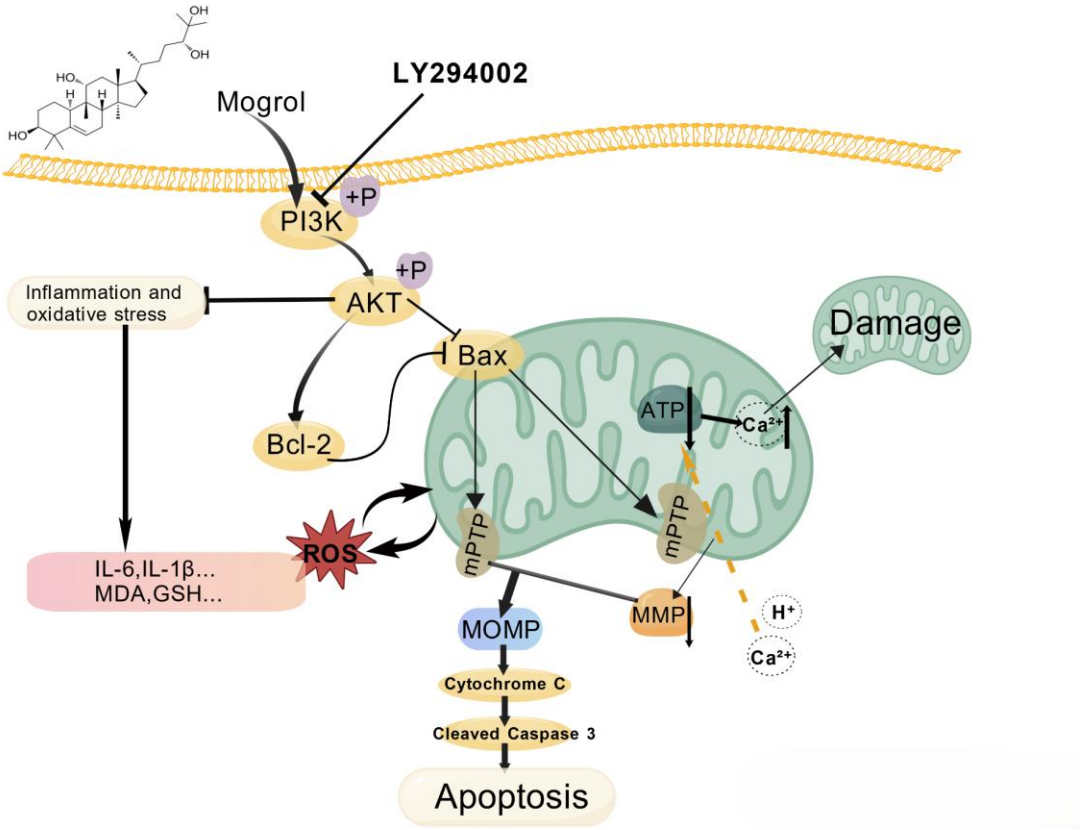


Figure9 Schematic illustration of the mechanism underlying the protective effects of Mogrol in HIRI.

Class I PI3K represents a heterodimeric complex composed of a catalytic subunit

(p110) and a regulatory subunit (p85). AKT functions as a downstream effector of Class I PI3K, and phosphorylated AKT participates in regulating the activity of diverse substrates that are essential for cellular survival, cell cycle progression, and cellular proliferation(43). Previous investigations have established that the PI3K/AKT signaling cascade demonstrates critical importance in HIRI pathogenesis(29). The Bcl-2 protein family functions as a downstream effector of the PI3K/AKT signaling cascade(44). Upon AKT activation, Bcl-2 expression increases whereas Bax expression decreases(45). In this investigation, we observed that Mogrol prophylactic treatment enhanced Bcl-2 expression and diminished Bax expression. This reduction decreased the quantities of cytochrome c and the downstream cleaved caspase-3 proteins, consequently suppressing mitochondrial-mediated apoptosis. However, the way in which Mogrol influences the expression of these apoptotic proteins is still not understood. Combined transcriptomic and bioinformatics analyses implicated the PI3K/AKT signaling pathway as a major contributor to the protective effects of Mogrol in HIRI. In agreement with this, molecular docking revealed strong binding to the PI3K p85 subunit, and subsequent western blot analysis provided experimental validation. In the end, we added LY294002 to verify the protective mechanism of Mogrol's effect on HIRI. Under conditions without LY294002 intervention, Mogrol pretreatment promoted PI3K/AKT pathway activation and was associated with inhibition of mitochondria-dependent apoptosis, as well as decreased oxidative stress and inflammation. However, after the addition of LY294002, the safeguarding effect of Mogrol on HIRI was significantly reversed.

5. Conclusion

In conclusion, Mogrol attenuates HIRI in experimental models by suppressing oxidative injury, mitochondrial dysfunction, and apoptosis. Thus, Mogrol represents a potential therapeutic candidate for HIRI.

Ethics approval

Animal experiments were conducted strictly in accordance with the ARRIVE guidelines and followed the National Research Council's guidelines for the care and use of laboratory animals. This study has been approved by the Ethics Committee of the First Affiliated Hospital of Zhengzhou University. (2023-KY-0761-002).

Consent for publication

Not applicable.

Data Sharing Statement

The data underlying this article will be shared upon reasonable request by the corresponding author.

Conflict of interest

The authors declare no conflicts of interest regarding the publication of this article.

Funding.

This study was supported by grants from the National Natural Science Foundation of China (grant no. U2004122,81701946) and the Henan Charity Federation Fund (GDXZ2023014）.

CRediT authorship contribution statement.

Wenzheng Ruan: Writing – original draft, Project administration, Methodology. **Ying Zhu:** Data curation, Methodology. **An Zhao**: Project administration, Data curation. **Haoran Fang**: Software. **Qiwen Yu**: Methodology. **Shengli Cao**: Supervision, Funding acquisition.

Acknowledgements

We would like to express our gratitude to those who have provided assistance and support for this research.

References

1. Liu J, Luo R, Zhang Y, Li X. Current status and perspective on molecular targets and therapeutic intervention strategy in hepatic ischemia-reperfusion injury. Clin Mol Hepatol. 2024;30(4):585-619.
2. Hirao H, Nakamura K, Kupiec-Weglinski JW. Liver ischaemia-reperfusion injury: a new understanding of the role of innate immunity. Nat Rev Gastroenterol Hepatol. 2022;19(4):239-56.
3. Peralta C, Jimenez-Castro MB, Gracia-Sancho J. Hepatic ischemia and reperfusion injury: effects on the liver sinusoidal milieu. J Hepatol. 2013;59(5):1094-106.
4. Cannistra M, Ruggiero M, Zullo A, Gallelli G, Serafini S, Maria M, et al. Hepatic ischemia reperfusion injury: A systematic review of literature and the role of current drugs and biomarkers. Int J Surg. 2016;33 Suppl 1:S57-70.
5. Mukhopadhyay P, Horvath B, Zsengeller Z, Batkai S, Cao Z, Kechrid M, et al. Mitochondrial reactive oxygen species generation triggers inflammatory response and tissue injury associated with hepatic ischemia-reperfusion: therapeutic potential of mitochondrially targeted antioxidants. Free Radic Biol Med. 2012;53(5):1123-38.
6. R GB, Panisello-Rosello A, Sanchez-Nuno S, Alva N, Rosello-Catafau J, Carbonell T. Nrf2 and oxidative stress in liver ischemia/reperfusion injury. FEBS J. 2022;289(18):5463-79.
7. Li J, Li J, Fang H, Yang H, Wu T, Shi X, et al. Isolongifolene alleviates liver ischemia/reperfusion injury by regulating AMPK-PGC1α signaling pathway-mediated inflammation, apoptosis, and oxidative stress. International Immunopharmacology. 2022;113.
8. Khatun J, Gelles JD, Chipuk JE. Dynamic death decisions: How mitochondrial dynamics shape cellular commitment to apoptosis and ferroptosis. Dev Cell. 2024;59(19):2549-65.
9. Vringer E, Tait SWG. Mitochondria and cell death-associated inflammation. Cell Death Differ. 2023;30(2):304-12.
10. Nguyen TT, Wei S, Nguyen TH, Jo Y, Zhang Y, Park W, et al. Mitochondria-associated programmed cell death as a therapeutic target for age-related disease. Exp Mol Med. 2023;55(8):1595-619.
11. Bock FJ, Tait SWG. Mitochondria as multifaceted regulators of cell death. Nat Rev Mol Cell Biol. 2020;21(2).
12. Liu D, Liu Z, Hu Y, Xiong W, Wang D, Zeng Z. MOMP: A critical event in cell death regulation and anticancer treatment. Biochim Biophys Acta Rev Cancer. 2025;1880(2):189280.

13. Green DR. The Mitochondrial Pathway of Apoptosis: Part I: MOMP and Beyond. Cold Spring Harb Perspect Biol. 2022;14(5).
14. Yang H, Zhang P, Wang Q, Cheng K, Zhao Y. The research development of STAT3 in hepatic ischemia-reperfusion injury. Front Immunol. 2023;14:1066222.
15. Deng RM, Zhou J. Targeting NF-kappaB in Hepatic Ischemia-Reperfusion Alleviation: from Signaling Networks to Therapeutic Targeting. Mol Neurobiol. 2024;61(6):3409-26.
16. Yu B, Zhang Y, Wang T, Guo J, Kong C, Chen Z, et al. MAPK Signaling Pathways in Hepatic Ischemia/Reperfusion Injury. J Inflamm Res. 2023;16:1405-18.
17. Chen RX, Jiang WJ, Liu SC, Wang ZY, Wang ZB, Zhou T, et al. Apolipoprotein A-1 protected hepatic ischaemia-reperfusion injury through suppressing macrophage pyroptosis via TLR4-NF-kappaB pathway. Liver Int. 2023;43(1):234-48.
18. Glaviano A, Foo ASC, Lam HY, Yap KCH, Jacot W, Jones RH, et al. PI3K/AKT/mTOR signaling transduction pathway and targeted therapies in cancer. Mol Cancer. 2023;22(1):138.
19. Li H, Chen Y, Ding M, Yan Z, Guo W, Guo R. Pectolinarigenin attenuates hepatic ischemia/reperfusion injury via activation of the PI3K/AKT/Nrf2 signaling pathway. Chem Biol Interact. 2023;386:110763.
20. Rezq S, Hassan R, Mahmoud MF. Rimonabant ameliorates hepatic ischemia/reperfusion injury in rats: Involvement of autophagy via modulating ERK- and PI3K/AKT-mTOR pathways. International Immunopharmacology. 2021;100:108140.
21. Zhan M, Liu D, Yao L, Wang W, Zhang R, Xu Y, et al. Gas6/AXL Alleviates Hepatic Ischemia/Reperfusion Injury by Inhibiting Ferroptosis via the PI3K/AKT Pathway. Transplantation. 2024;108(11):e357-e69.
22. Liu Y, Gong S, Li K, Wu G, Zheng X, Zheng J, et al. Coptisine protects against hyperuricemic nephropathy through alleviating inflammation, oxidative stress and mitochondrial apoptosis via PI3K/Akt signaling pathway. Biomedicine & Pharmacotherapy. 2022;156.
23. Liang H, Cheng R, Wang J, Xie H, Li R, Shimizu K, et al. Mogrol, an aglycone of mogrosides, attenuates ulcerative colitis by promoting AMPK activation. Phytomedicine. 2021;81:153427.
24. Chen Y, Zhang L, Li Z, Wu Z, Lin X, Li N, et al. Mogrol Attenuates Osteoclast Formation and Bone Resorption by Inhibiting the TRAF6/MAPK/NF-kappaB Signaling Pathway In vitro and Protects Against Osteoporosis in Postmenopausal Mice. Front Pharmacol. 2022;13:803880.
25. Wang F, Zhou J, Liu W, Wang W, Tian B, Liu J, et al. Mogrol Regulates the Expression of ATPase Na+/K+ Transport Subunit 3, Inhibits Cardiomyocyte Apoptosis, and Plays a Protective Role Against Myocardial Infarction. Drug Design, Development and Therapy. 2025;Volume 19:1489-502.
26. Li H, Liu L, Chen HY, Yan X, Li RL, Lan J, et al. Mogrol suppresses lung cancer cell growth by activating AMPK-dependent autophagic death and inducing p53-dependent cell cycle arrest and apoptosis. Toxicol Appl Pharmacol. 2022;444:116037.
27. Tanaka C, Harada N, Teraoka Y, Urushizaki H, Shinmori Y, Onishi T, et al. Mogrol

stimulates G-protein-coupled bile acid receptor 1 (GPBAR1/TGR5) and insulin secretion from pancreatic beta-cells and alleviates hyperglycemia in mice. Sci Rep. 2024;14(1):3244.
28. Li R, Yan X, Xiao C, Wang T, Li X, Hu Z, et al. FTO deficiency in older livers exacerbates ferroptosis during ischaemia/reperfusion injury by upregulating ACSL4 and TFRC. Nat Commun. 2024;15(1):4760.
29. Zhang R, Zhang L, Manaenko A, Ye Z, Liu W, Sun X. Helium preconditioning protects mouse liver against ischemia and reperfusion injury through the PI3K/Akt pathway. J Hepatol. 2014;61(5):1048-55.
30. Li S, Yi Z, Deng M, Scott MJ, Yang C, Li W, et al. TSLP protects against liver I/R injury via activation of the PI3K/Akt pathway. JCI Insight. 2019;4(22).
31. Rabie MA, Zaki HF, Sayed HM. Telluric acid ameliorates hepatic ischemia reperfusion-induced injury in rats: Involvement of TLR4, Nrf2, and PI3K/Akt signaling pathways. Biochem Pharmacol. 2019;168:404-11.
32. Lin J, Li F, Jiao J, Qian Y, Xu M, Wang F, et al. Quercetin, a natural flavonoid, protects against hepatic ischemia-reperfusion injury via inhibiting Caspase-8/ASC dependent macrophage pyroptosis. J Adv Res. 2025;70:555-69.
33. Li J, Yu D, He C, Yu Q, Huo Z, Zhang Y, et al. KLF6 alleviates hepatic ischemia-reperfusion injury by inhibiting autophagy. Cell Death Dis. 2023;14(7):393.
34. George J, Lu Y, Tsuchishima M, Tsutsumi M. Cellular and molecular mechanisms of hepatic ischemia-reperfusion injury: The role of oxidative stress and therapeutic approaches. Redox Biology. 2024;75.
35. Du S, Zhang X, Jia Y, Peng P, Kong Q, Jiang S, et al. Hepatocyte HSPA12A inhibits macrophage chemotaxis and activation to attenuate liver ischemia/reperfusion injury via suppressing glycolysis-mediated HMGB1 lactylation and secretion of hepatocytes. Theranostics. 2023;13(11):3856-71.
36. Liu J, Man K. Mechanistic Insight and Clinical Implications of Ischemia/Reperfusion Injury Post Liver Transplantation. Cell Mol Gastroenterol Hepatol. 2023;15(6):1463-74.
37. Sun Q, Yang R, Chen T, Li S, Wang H, Kong D, et al. Icaritin attenuates ischemia-reperfusion injury by anti-inflammation, anti-oxidative stress, and anti-autophagy in mouse liver. Int Immunopharmacol. 2024;138:112533.
38. Tang SP, Mao XL, Chen YH, Yan LL, Ye LP, Li SW. Reactive Oxygen Species Induce Fatty Liver and Ischemia-Reperfusion Injury by Promoting Inflammation and Cell Death. Front Immunol. 2022;13:870239.
39. Jaiswal V, Lee HJ. Pharmacological Activities of Mogrol: Potential Phytochemical against Different Diseases. Life (Basel). 2023;13(2).
40. Machado IF, Palmeira CM, Rolo AP. Preservation of Mitochondrial Health in Liver Ischemia/Reperfusion Injury. Biomedicines. 2023;11(3).
41. Zhang S, Rao S, Yang M, Ma C, Hong F, Yang S. Role of Mitochondrial Pathways in Cell Apoptosis during He-Patic Ischemia/Reperfusion Injury. Int J Mol Sci. 2022;23(4).
42. Huang J, Xie P, Dong Y, An W. Inhibition of Drp1 SUMOylation by ALR protects the liver from ischemia-reperfusion injury. Cell Death Differ. 2021;28(4):1174-92.

43. Fresno Vara JA, Casado E, de Castro J, Cejas P, Belda-Iniesta C, Gonzalez-Baron M. PI3K/Akt signalling pathway and cancer. Cancer Treat Rev. 2004;30(2):193-204.
44. Chen K, Li Y, Zhang X, Ullah R, Tong J, Shen Y. The role of the PI3K/AKT signalling pathway in the corneal epithelium: recent updates. Cell Death Dis. 2022;13(5):513.
45. Ren C, Ren T, Yang K, Wang S, Bao X, Zhang F, et al. Inhibition of SOX2 induces cell apoptosis and G1/S arrest in Ewing's sarcoma through the PI3K/Akt pathway. J Exp Clin Cancer Res. 2016;35:44.

Supplementary Files

This is a list of supplementary files associated with this preprint. Click to download.

- Supplementarymaterials.docx